

Numerical analysis of concrete degradation due to chloride-induced steel corrosion

Olawale O. Ayinde, Xiao-Bao Zuo* and Guang-Ji Yin

Department of Civil Engineering, School of Science, Nanjing University of Science and Technology, 210094, Nanjing, China

(Received February 5, 2018, Revised January 25, 2019, Accepted March 17, 2019)

Abstract. Concrete structures in marine environment are susceptible to chloride attack, where chloride diffusion results in the corrosion of steel bar and further lead to the cracking of concrete cover. This process causes structural deterioration and affects the response of concrete structures to different forms of loading. This paper presents the use of ABAQUS Finite Element Software in simulating the processes involved in concrete's structural degradation from chloride diffusion to steel corrosion and concrete cover cracking. Fick's law was used for the chloride diffusion, while the mass loss from steel corrosion was obtained using Faraday's law. Pressure generated by steel corrosion product at the concrete-steel interface was modeled by applying uniform radial displacements, while concrete smeared cracking alongside the Extended Finite Element Method (XFEM) was used for concrete cover cracking simulation. Results show that, chloride concentration decreases with penetration depth, but increases with exposure time at the concrete-steel interface. Cracks initiate and propagate in the concrete cover as pressure caused by the steel corrosion product increases. Furthermore, the crack width increases with the exposure time on the surface of the concrete.

Keywords: concrete; steel; chloride; corrosion; cracking; extended finite element method; ABAQUS

1. Introduction

Chloride attack is a threat to the durability of onshore and offshore structures, exposed to marine environment over time, due to the combined action of physical and chemical processes (Ashish *et al.* 2016). Chloride ion in seawater diffuses into concrete through the concrete cover, and accumulate at the concrete-steel interface until its concentration reaches a critical value, resulting in the depassivation and corrosion of steel bar. The steel corrosion causes the loss of steel sectional area, the degradation of bond between steel and concrete, enhances structural deflection, as well as the cracking of concrete cover (Wong *et al.* 2010, Zhu and Francois 2013, Zhou *et al.* 2019). Corrosion of steel bar and its induced degradation of concrete can cause a reduction in the bearing capacity of concrete structures, and further decrease their service performances. Thus, an analysis of steel corrosion and its induced concrete degradation during chloride attack is very necessary to investigate the durability degradation of reinforced concrete (RC) exposed to marine environments.

Chloride-induced steel corrosion can change the bond property between steel bar and concrete in RC structures (Fang *et al.* 2006, Coccia *et al.* 2016). A limited amount of steel corrosion can increase the roughness of the steel surface (Lee *et al.* 2004), and improve bond strength of reinforced concrete (Auyeung *et al.* 2000), However, as steel corrosion increases, the corrosion products will cause

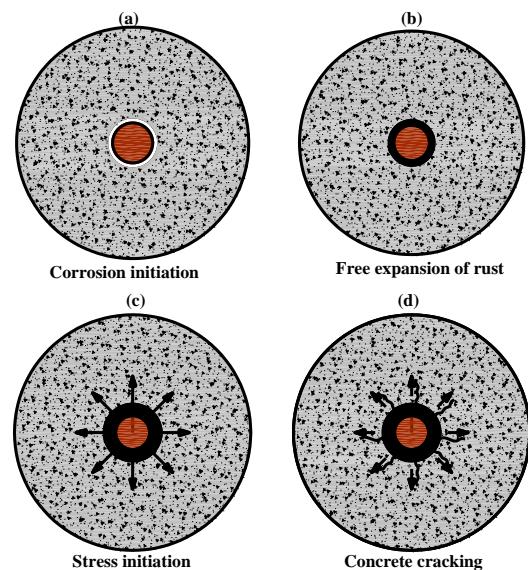


Fig. 1 Chloride-induced steel corrosion and concrete cracking (Chen and Mahadevan 2008)

a gradual reduction in bond property, and produce the tensile stress exerted on the concrete cover because of its volume expansion, which is about two to six times that of the sound steel (Zhao *et al.* 2016). The steel corrosion products generate tensile stresses in the concrete, and when the tensile stress increases to a level, it causes crack formation and propagation in the concrete cover. A pictorial representation of these processes is shown in Fig. 1.

Many models have been proposed to describe the cracking process of concrete, due to the corrosion of steel

*Corresponding author, Professor
E-mail: xbzuo@sina.com

bar. As stated by Val *et al.* (2009), one of the earliest analytical models was proposed by Bazant (1979), to determine the time of concrete cover cracking. Experiments have been conducted to establish the critical value of steel corrosion needed for concrete cracking, and to determine the parameters that influence this value, alongside proposing some valuable empirical models (Williamson and Clark 2000, Val *et al.* 2009). Vidal *et al.* (2004)'s research links the amount of steel corrosion with the width of concrete cracks. Empirical models have also been used to determine the rate of chloride-induced steel corrosion in concrete. These empirical models are often based on the analysis of experimental results for the determination of influential parameters in concrete cover cracking, including geometric parameters, like concrete cover thickness, steel bar diameter, and the concrete property (Vu and Stewart 2000, Vu *et al.*, 2005, Guo *et al.* 2015, Otieno *et al.* 2016, Lu *et al.* 2018). Furthermore, Williamson and Clark (2000) highlighted that linear relationships have often been obtained between the amount of steel corrosion and the crack width of concrete for most of the experimental studies.

Based on the thick-walled cylinder approach, some analytical models on concrete cover cracking were proposed by Bazant (1979), Liu and Weyers (1998), in which an internal circular boundary condition exists between concrete and steel bar, and it is displaced to allow for the expansive nature of the corrosion products. The difference between these models is the recognition of the presence of a porous zone at the concrete-steel interface by Liu and Weyers (1998), as well as the addition of varying rust formation which was initially assumed constant by Bazant (1979). A number of analytical and numerical investigations on the steel corrosion-induced cracking of concrete cover have also been conducted, such as in the research of Xiao *et al.* (2001), Du *et al.* (2006), Otieno *et al.* (2011), Lu *et al.* (2011), Sanz *et al.* (2013), Zhao *et al.* (2016). Chen and Mahadevan (2008) employed numerical tools to simulate the chloride-induced degradation process of RC structures. Pantazopoulou and Papoulia (2001) also presented a numerical model for concrete cover cracking, considering the partition of the cylinder into a cracked and uncracked part, as well as the change in secant stiffness of concrete. Chernin and Val (2011) presented a numerical study of the concrete cover cracking using a thermal analogy to determine the expansive nature of corrosion products in concrete.

At present, most studies on the steel corrosion-induced concrete cracking in the cover have employed different 2D constitutive models with plane strain formulation. However, as indicated by Val *et al.* (2009), a poor agreement has often been noticed between the Finite Element analysis and experimental results, due to the lack of a chloride diffusion result that considers many diffusive environmental factors, as well as inadequate knowledge of the movement of corrosion products into concrete pores. This paper presents the use of the Finite Element Method in simulating the processes involved in concrete degradation due to chloride-induced steel corrosion, considering a temperature-dependent chloride diffusion. Steel corrosion due to the chloride concentration at the concrete-steel interface is

evaluated. Concrete cover cracking resulting from the expansive nature of steel-corroded products was established by using the ABAQUS XFEM.

2. Chloride diffusion in concrete

The diffusion mechanism describes the complex physio-chemical process of the movement of chloride into concrete (Muthulingam and Rao 2014), affected by various diffusive factors, and with high degree of nonlinearity. According to Zehtab and Tarighat (2016), the diffusion process depends on the reactivity of ions, their concentrations and the diffusion coefficients. Chloride diffusion takes place in a saturated concrete, and it is usually characterized by Fick's second law, given as

$$C(x,t) = C_0 \left\{ 1 - \operatorname{erf} \left[\frac{x}{2\sqrt{Dt}} \right] \right\} \quad (1)$$

where $C(x,t)$ represents the chloride concentration (kg/m^3) at depth $x(\text{m})$ of chloride penetration and time t (yrs.). C_0 is the constant surface chloride concentration, and D represents the apparent diffusion constant ($\text{m}^2/\text{yr.}$).

The diffused chloride ions are divided into free and bound chlorides in concrete, but the steel corrosion is only caused by the free chloride ions, while the bound chlorides are deducted from the diffusion equation (Zhou *et al.* 2019). When the chloride concentration at the concrete-steel interface exceeds the chloride threshold for depassivation, steel corrosion is initiated in the passive protective zone at the concrete-steel interface. According to Glass and Buenfeld (1997), the chloride threshold for depassivation is distributed within the range of 0.17% and 1.4% by weight of cement on U.S. bridges, while similar values between 0.2% and 1.5% are reported for U.K bridges representing minimal corrosion and very high corrosion risk, respectively. In this study, the depassivated chloride threshold of 0.5% by wt. of cement (1.75 kg/m^3), is chosen to indicate normal corrosion.

2.1 Finite element analysis

The Finite Element Method can be used to determine the chloride diffusion in concrete, in which the influence of temperature is considered, using a transient analysis (Muthulingam and Rao 2014). The relationship between chloride diffusion and concrete temperature was established by Saetta *et al.* (1993); Tang and Nilsson (1994), Hansen and Saouma (1999). According to them, a decrease in concrete temperature leads to a reduction in chloride diffusivity, while Ashish *et al.* (2016) also emphasized that chemical attack increases in Temperature zones. The Arrhenius' Law given in Eq. (2) is the governing principle for the temperature-dependent chloride diffusivity in concrete.

$$D = D_0 \exp \left[\frac{E}{R} \left(\frac{1}{T_0} - \frac{1}{T} \right) \right] \quad (2)$$

where D_0 is the chloride diffusion constant, $\text{m}^2/\text{yr.}$, E is the activation energy of the chloride diffusion, $E=18.5\text{KJ/mol}$,

Table 1 Main parameters for numerical simulation

Heat transport	
Concrete Density,	$\rho_{\text{concrete}}=2400 \text{ kg/m}^3$
Specific heat,	$c=1000 \text{ J/(Kg.K)}$
Thermal Conductivity,	$D_{T, \text{concrete}}=2 \text{ W/(m.K)}$
Initial Temperature ,	$T_{\text{ini}}=293.65 \text{ K}$
Chloride transport	
Exposure time,	$t=100 \text{ years}$
Diffusivity,	$D_0=1.07224 \times 10^{-4} \text{ m}^2/\text{yr.}$
Solubility,	$s=1$
weight of cement,	$\text{wt.}=350 \text{ kg/m}^3$

R is the gas constant, $R=8.314 \text{ J/mol.K}$, T is the concrete temperature, K , T_0 is the temperature at which D_0 is determined. The temperature T at any given point in a concrete specimen can be obtained from the thermal analysis of the concrete section using Finite Element Analysis. According to Hansen and Saouma (1999), a numerical model for chloride diffusion in concrete can predict the time needed for the chloride concentration to reach its threshold at the concrete-steel interface.

In this study, an initially chloride-free reinforced concrete bridge pier is idealized as a cylindrical concrete section, modeled and solved using the Mass Diffusion algorithm of the ABAQUS software. The temperature-dependent chloride diffusion was conducted, with boundary conditions of constant surface chloride concentration, C_0 of 3.5 kg/m^3 and temperature, $T=288.9+11.15\sin(2\pi t)$, applied on the body surface, where t , is the exposed time in years. The heat transfer and chloride diffusion in concrete were first solved independently, then a temperature-dependent mass diffusion was carried out to obtain the spatial and time-dependent chloride concentration distribution in concrete. A Fick's law diffusion algorithm was used with the transient analysis conducted for an exposure time of 100 years, while an 8-node linear heat transfer element (DC3D8) was used in Finite element analysis. Main parameters used for the numerical simulation on the heat transfer and chloride diffusion are presented in Table 1.

2.2 Chloride diffusion FE results

From the Finite Element analysis of chloride diffusion in concrete, Fig. 2 shows the change of chloride concentration at the concrete-steel interface with the exposure time in the chloride environment. It can be observed from the figure that, for the first three years of chloride diffusion, there is no chloride concentration at the concrete-steel interface. After continuous exposure beyond the first three years, the chloride concentration gradually increases with the exposure time, towards reaching the value of the chloride concentration of 3.5 kg/m^3 at the concrete surface. This is because the chloride diffusion from the chloride environment needs three years to get to the steel bar surface. However, this concentration decreases with depth of penetration, as shown in Fig. 3. Due to the impermeability of steel bar, the diffused chloride ion accumulates at the steel bar surface with the time of chloride diffusion, and leads to the chloride concentration

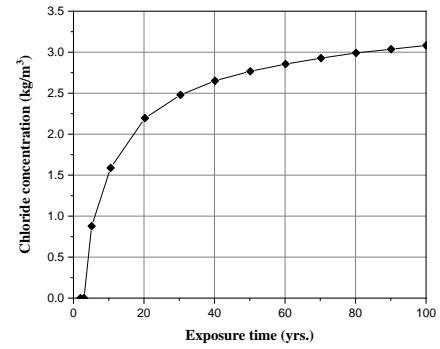


Fig. 2 Change of chloride concentration at the concrete-steel interface with exposure time

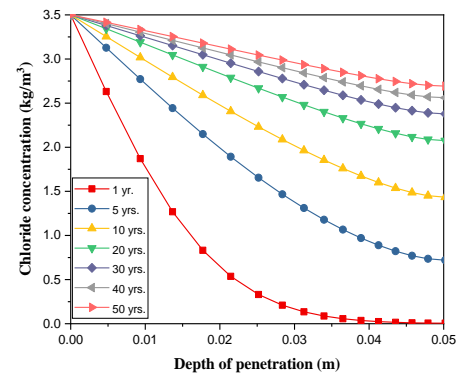


Fig. 3 Chloride concentration distribution at different exposure time

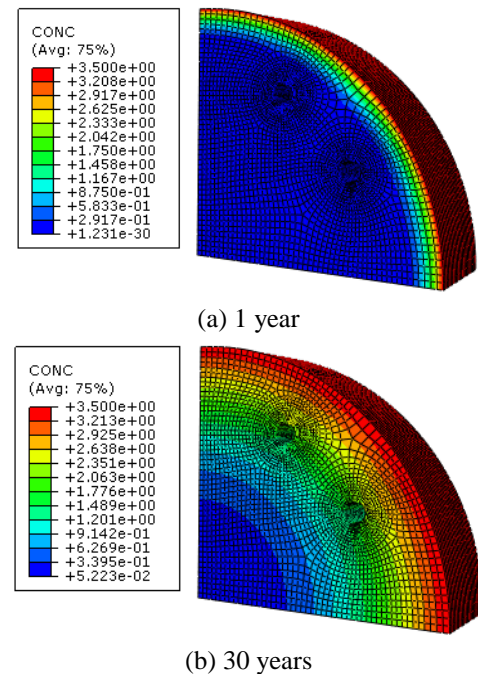


Fig. 4 Chloride concentration distribution obtained from FE analysis at different exposure time

reaching its threshold, in which the steel corrosion is assumed to begin. A chloride threshold of 1.75 kg/m^3 (0.5% by weight of cement) was obtained after 15 years of chloride diffusion, indicating the initiation of steel

corrosion.

Fig. 4 gives the distribution of the chloride concentration at different exposure times.

3. Steel corrosion in concrete

Corrosion of steel reinforcement is a complex electrochemical reaction that occurs due to the presence of chloride ion at the surface of the steel (Zhou *et al.* 2019). Steel corrosion causes the loss of the original mass and the reduction of the effective area of the steel bar. Generally, the mass loss of steel due to corrosion, is determined theoretically by using Faraday's law, expressed as (Fang *et al.* 2006)

$$M_{loss} = \frac{A \cdot I_{corr} \cdot t}{n \cdot F} \quad (3)$$

where M_{loss} represents the mass loss of steel bar due to corrosion, A is the atomic mass of the corroded steel, $A=55.847$ g/mol, I_{corr} represents the magnitude of electrical current, t is the active corrosion time, yrs., F is Faraday's constant, $F=96500$ C/mol, and n is the valency of the iron electron, usually taken as 2. The reduction in the diameter of steel bar and the increase in the volume of corrosion products are features that indicate corrosion of embedded steel bar. Based on Eq. (3), Pantazopolous and Papoulia (2001) presented a relation to obtain these parameters

$$D_{rb} = D_b - 0.023i_{corr}\Delta t \quad (4)$$

$$\Delta V_s = 0.0115\pi D_b i_{corr} \Delta t \quad (5)$$

where D_{rb} is the diameter of remaining steel bar, in meters, D_b is the original diameter of steel bar ($D_b=0.02$ m), in metres, i_{corr} is the steel corrosion rate, in $\mu\text{A}/\text{cm}^2$, Δt is the difference between the exposure and corrosion times, in years.

3.1 Steel corrosion rate

The steel corrosion rate is needed to estimate the change in volume of corrosion products and also to obtain the reduction in cross-sectional area of steel bar (Ožbolt *et al.* 2012). The constant and dynamic corrosion rates are used to determine the corrosion of steel bar in concrete subjected to chloride attack. Based on the assumption of a constant steel corrosion rate and corrosion product formation, some steel corrosion models have been successfully adopted by many researchers (Fang *et al.* 2006, Chen and Mahadevan 2008). In this study, the dynamic steel corrosion rate, given by Chen and Mahadevan (2008), is expressed as

$$i_{corr} = 0.926 \exp \left[7.98 + 0.777 \ln(1.69C_t) - \frac{3006}{T} - 0.000116R_c + 2.24t^{-0.215} \right] \quad (6)$$

where C_t is the total chloride concentration at the surface of steel bar, kg/m^3 , R_c is the ohmic resistance of concrete cover, ohms. Liu and Weyers (1998) obtained regression relationship between the total chloride content and ohmic resistance R_c , expressed as

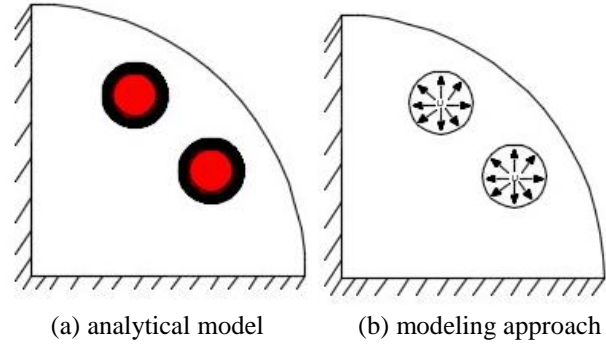


Fig. 5 Model of steel corrosion-induced expansion in concrete

$$R_c = \text{Exp} [8.03 - 0.549 \ln(1 + 1.69C_t)] \quad (7)$$

Pantazopolous and Papoulia (2001) presented the mass loss of steel bar per meter length

$$M_{loss} = 2.8951 \times 10^{-7} \pi D_b \Delta t \cdot i_{corr} \quad (8)$$

with M_{loss} given as the mass loss of steel, (kg/m).

3.2 Steel corrosion-induced expansive pressure

The effect of steel corrosion on concrete is the expansive stresses generated by its products. The expansive stresses at the concrete-steel interface was modeled by applying radial displacements on the concrete section, an approach supported by Du *et al.* (2006), Zhao and Jin (2006), Val *et al.* (2009) and Xiao *et al.* (2011). The applied radial displacements indicate an increase in the pressure exerted on the concrete cover with the exposure time at the concrete-steel interface, as presented in Fig. 9. This pressure causes crack formation and propagation in the concrete cover, which negatively affects the durability of concrete structures.

There exists a relationship between the radial displacement of concrete and corrosion pressure, and El-Maddawwy and Soudki (2007) presented a linear relationship between them, expressed as

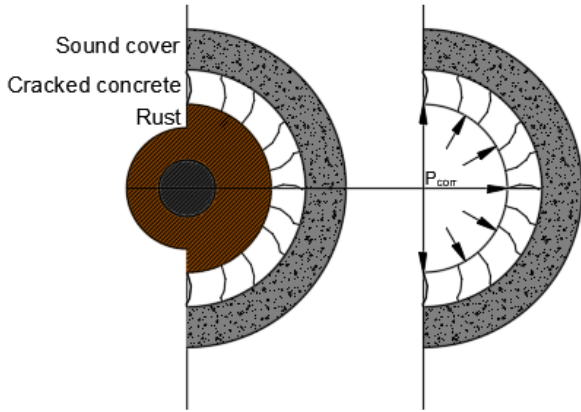
$$\delta_c = kP_{corr} \quad (9)$$

where δ_c is the radial displacement of concrete, m, P_{corr} is the steel corrosion-induced pressure, Pa, k is the hole flexibility constant, m/Pa, considering the initial filling of steel corrosion products in the porous zone at concrete-steel interface before the generation of expansive stress, and it is expressed by

$$k = \frac{(1 + \mu + \nu)(D_b + 2\delta_0)}{2E_{ef}} \quad (10)$$

μ is concrete's poisson ratio, E_{ef} is the effectively elastic modulus of concrete, Pa, δ_0 is the porous zone thickness, $\delta_0=12.5 \mu\text{m}$ (Liu and Weyers 1998, Val *et al.* 2009), ν is a dimensionless parameter which is associated with the concrete cover and the steel diameter, given as

$$\nu = \frac{(D_b + 2\delta_0)^2}{2C(C + D_b + 2\delta_0)} \quad (11)$$


 Fig. 6 Uniform cracking model (Cao *et al.* 2013)

C is the concrete cover, ($C=0.05$ m).

By using the obtained mass loss due to steel corrosion from Eq. (8), the pressure exerted on concrete by the radial expansion of the corrosion product is given as (El-Maddawwy and Soudki 2007)

$$P_{\text{corr}} = \frac{2E_{\text{ef}}}{(1+\mu+\nu)(D_b+2\delta_0)} \left[\frac{M_{\text{loss}}}{\pi D_b} \left(\frac{1}{0.622\rho_r} - \frac{1}{\rho_s} \right) - \delta_0 \right] \quad (12)$$

where ρ_r is the mass density of steel corrosion products, kg/m^3 , ρ_s is the mass density of steel, kg/m^3 , M_{loss} given as the mass loss of steel, (kg/m). Negative values of P_{corr} correspond to the time in which the corrosion products occupy the porous zone at the concrete-steel interface, which results in zero pressure, with zero displacement.

4. Cracking of concrete

With increase in steel corrosion-induced pressure on concrete, cracks occur on the inner and outer surfaces of concrete cover, until the cracks completely penetrate the concrete cover (Du *et al.* 2006). Crack is assumed to be formed when the observed crack width is approximately 0.05 mm (Val *et al.* 2009), after which cracks grow with increasing width and length. Cao *et al.* (2013) presents a typical uniform corrosion model, which is shown in Fig. 6.

4.1 Concrete fracture

The fracture of concrete can be described as a cohesive crack which opens while still transferring stress from one face to the other. The Hillerborg cohesive crack model (Hillerborg *et al.* 1976) defines the tension softening in the direction normal to a crack. The softening function, defined by tensile strength, f_t , MPa, and fracture energy, G_F , J/m^2 , can reflect the tensile behavior of concrete (Guinea 1995). The crack width is another factor that governs the fracture mechanics using the Hillerborg cohesive crack model, as presented in Fig. 7. A simple relation given by Hillerborg *et al.* (1976) for the cohesive crack model is expressed as

$$\int_0^{w_c} \sigma dw = \frac{f_t w_c}{2}, \quad w = \frac{2G_F}{f_t} \quad (13)$$

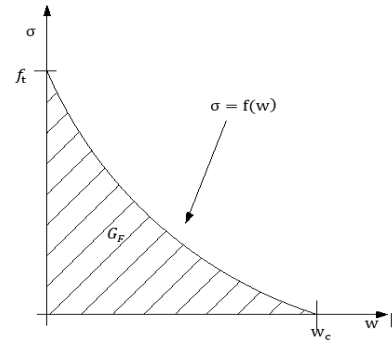


Fig. 7 Hillerborg softening curve (Guinea 1995)

where σ is the stress transferred to the crack, Pa, w is the crack width, m, and w_c is the critical crack opening at which the stress transferred becomes zero, m.

4.2 Numerical simulation of cracking

The non-linear analysis of concrete cracking was performed by using the concrete smeared cracking approach, for different levels of expansion caused by the steel corrosion products. Crack formation and propagation are considered as a two-dimensional plain-strain problem formulation, which is idealized as a cylindrical concrete model and solved in ABAQUS Finite Element Analysis software. With concrete represented as an 8-node linear brick element, with reduced integration and hourglass control (C3D8R), a uniform radial displacement was applied on the concrete to simulate the pressure exerted by corrosion products. The concrete properties include, density, $\rho=2400$ kg/m^3 , Poisson ratio $\mu=0.15$, Elastic Modulus $E=31.0$ GPa, Tensile strength $f_t=3.00$ MPa, and compressive strength $f_c=15.0$ MPa.

Cracking of concrete caused by steel corrosion was modeled by using the Extended Finite Element Method (XFEM), which allows the easy incorporation of local enrichment functions into a finite element approximation. This method alleviates the shortcomings of the regular finite element method, and it has advantages of easier crack definition, improved convergence rates for stationary cracks and simplified mesh refinement studies.

As given by the Hillerborg cohesive crack model and implemented in the ABAQUS software, crack width and propagation pattern is influenced by the Fracture Energy, G_F . This however gives an indication that the crack is not produced until the fracture energy is reached for visible fracture (crack) to occur in the concrete element. By employing the concrete smeared cracking approach with the Extended Finite Element Method in ABAQUS, the crack initiation and propagation is modelled and solved. The numerical simulation data include the Maximum Principal stress, $\text{MAXPS}=3.00$ MPa, the fracture energy, $G_F=75$ J/m^2 , with crack stabilization of 1.0×10^{-6} , which aids the stiffness of the structure and helps with convergence.

Fig. 8 shows the result of the numerical simulation of the cracking of concrete caused by steel corrosion, where vertical cracks initiate in concrete and propagate vertically with increasing length and width. Alongside the main

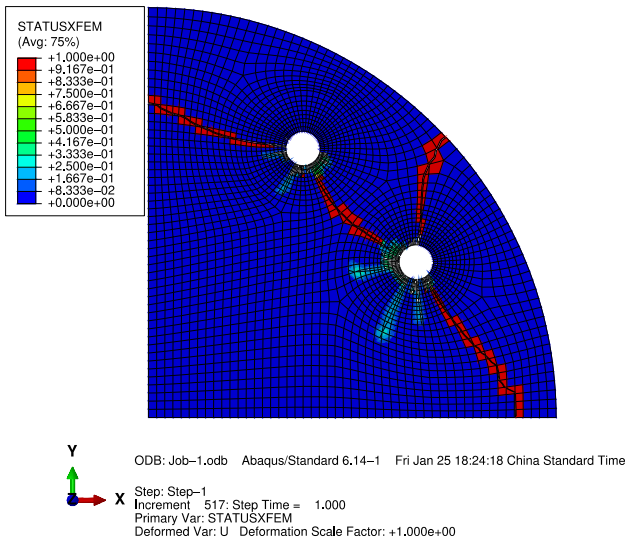


Fig. 8 Main crack propagating from the concrete-steel interface alongside other cracks

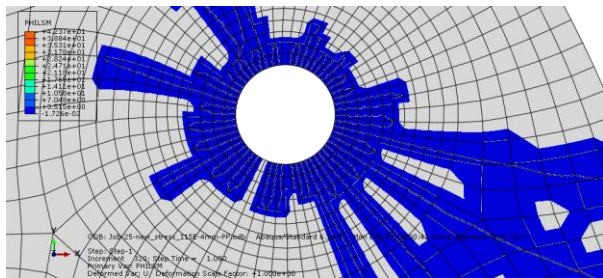
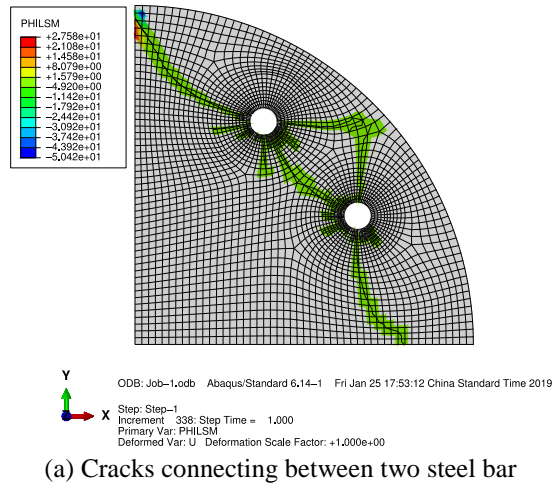
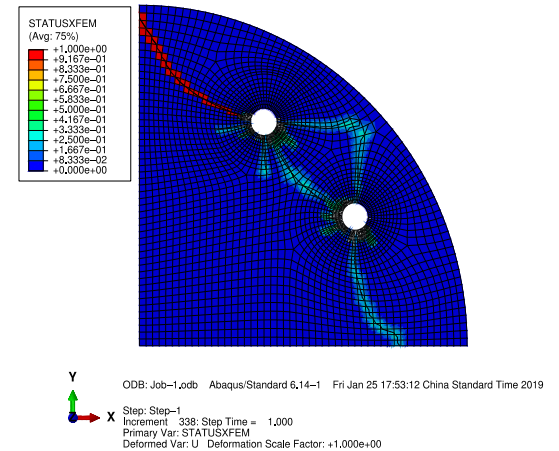


Fig. 9 Inclined cracks shown around the concrete-steel interface



(a) Cracks connecting between two steel bar



(b) STATUS XFEM revealing the delamination layer

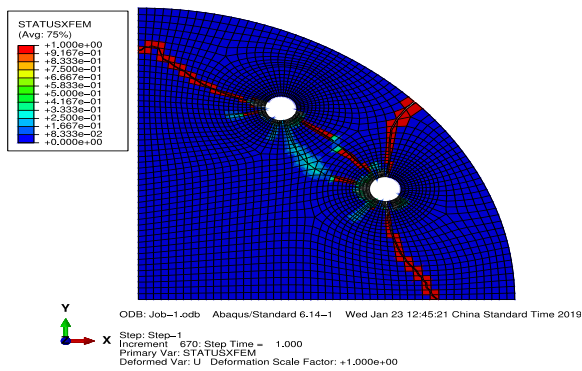
Fig. 10 Delamination layer formed by the connection of cracks between the reinforcements

vertical cracks, other smeared cracks appear along the concrete-steel interface, but do not propagate to the extent of the main cracks. The number of the observed main cracks are subjected to discussion, but as seen from the figure, a good cracking pattern is obtained. After the cracks are first formed in the concrete members close to the concrete-steel interface, the concrete member allows the propagation of these cracks to other joint members, as discretized in the model.

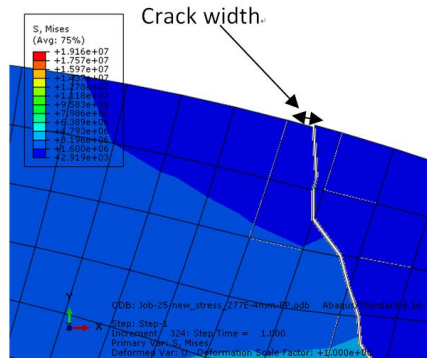
In line with the main cracks that propagate, other radial cracks inclined either 45° or 90° to the main crack, also propagate, which is in agreement with the observation of Val *et al.* (2009), Xiao *et al.* (2011). These inclined cracks are obvious in all of the cracking patterns, as presented in Fig. 9. The propagation path and rate of propagation of the main cracks are however different. Some cracks propagated rapidly, while some propagated at a relatively reduced rate. Dagher and Kulendran (1992), from their experimental result, explained that cracks may propagate and connect between the steel bars and form a delamination layer inside a concrete element, if the steel bars are closely spaced and with thick concrete cover. With such a delamination, the concrete element becomes unstable, with a rapid release of the accumulated expansive stress in concrete. Similar situation was experienced in the results from the simulation as cracks propagated and connected between two closely placed steel bar, as shown in Fig. 10.

Another visible observation from the delaminated layer is that the stress in the crack zone goes to a negative value which can be taken as zero. The fracture energy has been completely used up and the stress is now transferred over the aggregates or the corrosion products that exist between the cracks. With increase in the radial expansion of corrosion products, cracks occur at the inner surface of the concrete cover and at the location of the maximum radial expansion, which is in accordance with the used Hillerborg cohesive crack model. Du *et al.* (2006) however, referred to such cracks as internal cracking. These internal cracks increase in an inhomogeneous manner in length and width until it reaches the concrete surface. The crack width can be determined when the internally generated crack propagate to the surface of the concrete cover. Fig. 11 presents the observed crack width measurement in the XFEM model. As noted by Val *et al.* (2009), crack is said to be initiated in the concrete cover when the crack width is 0.05mm.

With increase in corrosion comes greater production of corrosion products as well as generation of higher tensile stresses in the concrete cover. This increase in tensile stress leads to increased pressure on the concrete cover obtained as increased radial displacement. In the numerical simulation, radial displacements beyond 8.50×10^{-6} m obtained after 55 years of corrosion gave mesh sensitivity



(a) Crack propagation up till the surface concrete cover



(b) Observed crack width

Fig. 11 Determination of the crack widths in XFEM model

and convergence problems. This is because when the tensile stress reaches its limit strength, the softening path becomes inadequate to model the non-linear behavior in a concrete element (Du *et al.* 2006). Fig. 12 shows the change of the crack width and radial displacement in the concrete cover with the exposure time in chloride environments. It can be seen from this figure that, the crack width and radial displacement increase linearly with the exposure time, but the rate of the increase of the crack width is higher when compared to the radial displacements. The result obtained is in agreement with the work of Andrade *et al.* (1993) who also obtained a linear variation between the crack width and volume of corrosion products, providing a viable basis for the result obtained.

5. Conclusions

This paper presents the numerical simulation of chloride-induced concrete deterioration processes. A temperature-dependent chloride diffusion was conducted using the Fick's law mass diffusion algorithm in ABAQUS FEM solver. The steel corrosion and corrosion product expansion were also modelled, while concrete cover cracking was simulated using ABAQUS XFEM algorithm. Results from the analysis are presented below:

- The chloride diffusion analysis shows a decrease in chloride concentration with depth of penetration. However, the chloride concentration at the concrete-steel interface increases with diffusion time due to the passive protective film located around the steel.

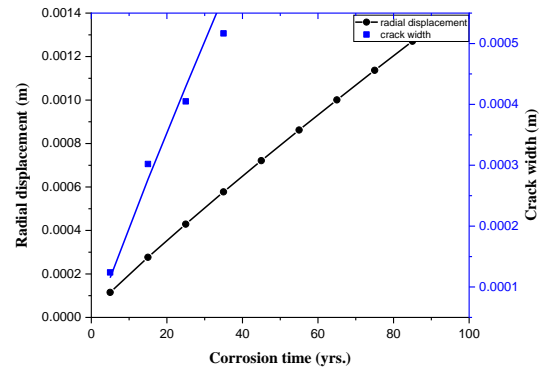


Fig. 12 Crack width and radial displacement with exposure time

- The steel corrosion analysis shows the mass loss result linearly varying with corrosion time. The corrosion pressure also varied linearly with corrosion time.
- The corrosion pressure increased with corrosion time, so also, the radial displacement in the concrete.
- The crack formation and propagation patterns for different values of applied radial displacement show an increasing length and width of cracks with increase in corrosion pressure.

Acknowledgment

This study was financially supported by National Science Foundation of China (51778297, 51378262).

References

- Andrade, C., Alonso, C. and Maslehuddin, F.J. (1993), "Cover cracking as a function of bar corrosion: Part 1-Experimental test", *Mater. Struct.*, **26**(8), 453-464. <https://doi.org/10.1007/BF02472805>
- Ashish, D.K., Singh, B. and Verma, S.K. (2016), "The effect of attack of chloride and sulphate on ground granulated blast furnace slag concrete", *Adv. Concrete Constr.*, **4**(2), 107-121. <http://dx.doi.org/10.12989/acc.2016.4.2.107>
- Auyeung, Y.B., Balaguru, P. and Chung, L. (2000), "Bond behavior of corroded reinforcement bars", *ACI Mater. J.*, **97**(2), 214-220.
- Bazant, Z.P. (1979), "Physical model for steel corrosion in concrete sea Structures-Application", *J. Struct. Div.*, ASCE, **105**(6), 1155-1166.
- Cao, C., Cheung, M.M.S. and Chan, B.Y.B. (2013), "Modelling of interaction between corrosion-induced concrete cover crack and steel corrosion rate", *Corros. Sci.*, **69**(24), 97-109. <https://doi.org/10.1016/j.corsci.2012.11.028>
- Chen, D. and Mahadevan, S. (2008), "Chloride-induced reinforcement corrosion and concrete cracking simulation", *Cement Concrete Compos.*, **30**(3), 227-238. <https://doi.org/10.1016/j.cemconcomp.2006.10.007>
- Chernin, L. and Val, D.V. (2011), "Prediction of corrosion-induced cover cracking in reinforced concrete structures", *Constr. Build. Mater.*, **25**(4), 1854-1869. <https://doi.org/10.1016/j.conbuildmat.2010.11.074>
- Coccia, S., Imperatore, S. and Rinaldi, Z. (2016), "Influence of corrosion on the bond strength of steel rebars in concrete",

- Mater. Struct.*, **49**, 537-551. <https://doi.org/10.1617/s11527-014-0518-x>.
- Dagher, H.J. and Kulendran, S. (1992), "Finite element modeling of corrosion damage in concrete structures", *ACI Struct. J.*, **S67**(89), 699-708.
- Du, Y.G., Chan, A.H.C. and Clark, L.A. (2006), "Finite element analysis of the effects of radial expansion of corroded reinforcement", *Comput. Struct.*, **84**, 917-929. <https://doi.org/10.1016/j.compstruc.2006.02.012>.
- El-Maaddawy, T. and Soudki, K. (2007), "A model for prediction of time from corrosion initiation to corrosion cracking", *Cement Concrete Compos.*, **29**(3), 168-175. <https://doi.org/10.1016/j.cemconcomp.2006.11.004>.
- Fang, C., Lundgren, K., Plos, M. and Gylltoft, K. (2006), "Bond Behavior of corroded reinforcing steel bars in concrete", *Cement Concrete Res.*, **36**(10), 1931-1938. <https://doi.org/10.1016/j.cemconres.2006.05.008>.
- Glass, G.K. and Buenfeld, N.R. (1997), "The presentation of the chloride threshold level for corrosion of steel in concrete", *Corros. Sci.*, **39**(5), 1001-1013. [https://doi.org/10.1016/S0010-938X\(97\)00009-7](https://doi.org/10.1016/S0010-938X(97)00009-7).
- Guinea, G.V. (1995), "Modelling the fracture of concrete: the cohesive crack", *Mater. Struct.*, **28**(4), 187-194. <https://doi.org/10.1007/BF02473248>.
- Guo, Y., Trejo, D. and Yim, S. (2015), "New model for estimating the time-variant seismic performance of corroding RC bridge columns", *J. Struct. Eng.* **141**(6), 04014158. [https://doi.org/10.1061/\(ASCE\)ST.1943-541X.0001145](https://doi.org/10.1061/(ASCE)ST.1943-541X.0001145).
- Hansen, E. and Saouma, V. (1999), "Numerical simulation of concrete deterioration-Part I: Chloride diffusion", *ACI Mater. J.*, **96**(2), 173-180.
- Hillerborg, A., Modeer, M. and Petersson, P.E. (1976), "Analysis of crack formation and crack propagation in concrete by means of fracture mechanics and finite elements", *Cement Concrete Res.*, **6**(6), 773-782. [https://doi.org/10.1016/0008-8846\(76\)90007-7](https://doi.org/10.1016/0008-8846(76)90007-7).
- Lee, B.D., Kim, K.H., Yu, H.G. and Ah, T.S. (2004), "The effect of initial rust on the bond strength of reinforcement", *J. Civil Eng.*, KSCE, **8**(1), 35-41. <https://doi.org/10.1007/BF02829078>.
- Liu, Y. and Weyers, R.E. (1998), "Modelling the time-to-corrosion cracking in chloride contaminated reinforced concrete structures", *ACI Mater. J.*, **95**(6), 675-681.
- Lu, C., Jin, W. and Liu, R. (2011), "Reinforcement corrosion-induced cover cracking and its time prediction for reinforced concrete structures", *Corros. Sci.*, **53**(4), 1337-1347. <https://doi.org/10.1016/j.corsci.2010.12.026>.
- Lu, Z., Lun, P., Li, W., Luo, Z., Li, Y. and Liu, P. (2018), "Empirical model of corrosion rate for steel reinforced concrete structures in chloride-laden environments", *Adv. Struct. Eng.*, 1-17. <https://doi.org/10.1177/1369433218783313>.
- Muthulingam, S. and Rao, B.N. (2014), "Non-uniform time-to-corrosion initiation in steel reinforced concrete under chloride environment", *Corros. Sci.*, **82**, 304-315. <https://doi.org/10.1016/j.corsci.2014.01.023>.
- Otieno, M.B., Beushausen, H.D. and Alexander, M.G. (2011), "Modelling corrosion propagation in reinforced concrete structures-A critical review", *Cement Concrete Compos.*, **33**(2), 240-245. <https://doi.org/10.1016/j.cemconcomp.2010.11.002>.
- Otieno, M., Beushausen, H. and Alexander, M. (2016), "Chloride-induced corrosion of steel in cracked concrete-Part I: Experimental studies under accelerated and natural marine environments", *Cement Concrete Res.*, **79**, 373-385. <https://doi.org/10.1016/j.cemconres.2015.08.009>.
- Ožbolt, J., Orsanic, F. and Balabanic, G. (2012), "Modelling damage in concrete caused by corrosion of reinforcement: coupled 3D FE model", *Int. J. Fract.*, **178**, 233-244. <https://doi.org/10.1007/s10704-012-9774-3>.
- Pantazopoulou, S.J. and Papoulia, K.D. (2001), "Modeling of cover cracking due to reinforcement corrosion in R.C. structures", *J. Eng. Mech.*, **127**(4), 342-351. [https://doi.org/10.1061/\(ASCE\)0733-9399\(2001\)127:4\(342\)](https://doi.org/10.1061/(ASCE)0733-9399(2001)127:4(342)).
- Saetta, A., Scotta, R. and Vitaliani, R. (1993), "Analysis of chloride diffusion into partially saturated concrete", *ACI Mater. J.*, **90**(5), 441-451.
- Sanz, B., Planas, J. and Sancho, J.M. (2013), "An experimental and numerical study of the pattern of cracking of concrete due to steel reinforcement corrosion", *Eng. Fract. Mech.*, **114**, 26-41. <https://doi.org/10.1016/j.engfracmech.2013.10.013>.
- Tang, L. and Nilsson, L. (1994), "A numerical method for prediction of chloride penetration into concrete structures", *The Modeling of Micro-structure and its Potential for Studying Transport Properties and Durability*, France.
- Val, D.V., Chernin, L. and Stewart, M.G. (2009), "Experimental and numerical investigation of corrosion-induced cover cracking in reinforced concrete structures", *J. Struct. Eng.*, **135**(4), 376-385. [https://doi.org/10.1061/\(ASCE\)0733-9445\(2009\)135:4\(376\)](https://doi.org/10.1061/(ASCE)0733-9445(2009)135:4(376)).
- Vidal, T., Castel, A. and Francois, R. (2004), "Analyzing crack width to predict corrosion in reinforced concrete", *Cement Concrete Res.*, **34**(1), 165-174. [https://doi.org/10.1016/S0008-8846\(03\)00246-1](https://doi.org/10.1016/S0008-8846(03)00246-1).
- Vu, K.A.T. and Stewart, M.G. (2000), "Structural reliability of concrete bridges including improved chloride-induced corrosion models", *Struct. Saf.*, **22**(4), 313-333. [https://doi.org/10.1016/S0167-4730\(00\)00018-7](https://doi.org/10.1016/S0167-4730(00)00018-7).
- Vu, K., Stewart, M.G. and Mullard, J. (2005), "Corrosion-induced cracking: Experimental data and predictive models", *ACI Struct. J.*, **102**(5), 719-726.
- Williamson, S.J. and Clark, L.A. (2000), "Pressure required to cause cover cracking of concrete due to reinforcement corrosion", *Mag. Concrete Res.*, **6**(52), 455-467. <https://doi.org/10.1680/macrc.2000.52.6.455>.
- Wong, H.S., Zhao, Y.X., Karimi, A.R., Buenfeld, N.R. and Jin, W.L. (2010), "On the penetration of corrosion products from reinforcing steel into concrete due to chloride-induced corrosion", *Corros. Sci.*, **52**(7), 2469-2480. <https://doi.org/10.1016/j.corsci.2010.03.025>.
- Xiao, P., Yi, N., Li, G. and Wang, L. (2011), "Finite element analysis of expansive behavior due to reinforcement corrosion in RC structure", *Proc. Eng.*, **12**, 117-126.
- Zehtab, B. and Tarighat, A. (2016), "Diffusion study for chloride ions and water molecules in C-S-H gel in nano-scale using molecular dynamics: Case study of tobermorite", *Adv. Concrete Constr.*, **4**(4), 305-317. <https://doi.org/10.12989/acc.2016.4.4.305>.
- Zhao, Y.X. and Jin, W.L. (2006), "Modeling the amount of steel corrosion at the cracking of concrete cover", *Adv. Struct. Eng.*, **9**(5), 687-696. <https://doi.org/10.1260/136943306778827556>.
- Zhao, Y., Dong, J., Wu, Y. and Jin, W. (2016), "Corrosion-induced concrete cracking model considering corrosion product-filled paste at the concrete/steel interface", *Constr. Build Mater.*, **116**, 273-280. <https://doi.org/10.1016/j.conbuildmat.2016.04.097>.
- Zhou, X., Tu, X., Chen, A. and Wang, Y. (2019), "Numerical simulation approach for structural capacity of corroded reinforced concrete bridge", *Adv. Concrete Constr.*, **7**(1), 11-22. <https://doi.org/10.12989/acc.2019.7.1.011>.
- Zhu, W. and Francois, R. (2013), "Effect of corrosion pattern on the ductility of tensile reinforcement extracted from a 26-year-old corroded beam", *Adv. Concrete Constr.*, **1**(2), 121-136. <http://dx.doi.org/10.12989/acc2013.1.2.121>.